

COMPUTATIONAL MODELING ANALYSIS OF RADAR SCATTERING BY CLOTHING COVERED ARRAYS OF METALLIC BODY-WORN EXPLOSIVE DEVICES

A. Angell and C. Rappaport

The Gordon Center for Subsurface Sensing and Imaging Systems
(Gordon-CenSSIS)
Northeastern University
Boston, MA 02115, USA

Abstract—In this study, we address the problem of detecting body-worn improvised explosive devices (IEDs) from a safe distance using radar. We have used a finite difference frequency domain (FDFD) model to simulate the radar signature of a typical scenario for body-worn IEDs, and have analyzed wrinkled clothing as a possible source of clutter, as well as the possibility for uniform versus nonuniform array spacing of explosive-filled metal pipes. Our analysis shows distinct characteristics of the pipe backscattered farfield signal for uniformly spaced pipes, with no significant clutter added when the metallic pipe is covered with wrinkled clothing.

1. INTRODUCTION

While explosive devices have always been a formidable threat to civilians as well as the military, the use of body-worn explosives poses a greater threat than ever before. Ever shrinking in size, these improvised explosive devices (IEDs) hide under the clothing of suicide bombers. The very nature of their improvised creation with non-standard parts makes it difficult to detect IEDs, especially in a timely manner at a safe distance.

It is important to develop a sensor that can detect whether a person is wearing such an explosive device at sufficient distance to prevent him from entering populated or strategically important areas.

One possible sensor which can observe through clothing is radar. High frequency radar beams above 20 GHz can be launched from relatively small aperture antennas with sufficiently small beamwidths

to discriminate targets in azimuth at distances of up to 100 m. Radars can be made inexpensively and are safe and easy to use.

One typical feature of body-worn IEDs is that they often tend to have outer metallic shells, resembling pipes or tubes. The metal casing increases the explosive's damage potential by projecting high-velocity shrapnel, but it also provides a detection characteristic. Circular metal cylinders have strong radar cross sections, scattering incident RF plane waves with characteristic patterns.

Additional clutter is added to the problem by other objects, whether part of the explosives, or part of normal non-uniformity in clothing. Analysis has been done for the effects not only of objects added for increased damage with minimal effort, such as nails, but also the effects of varied clothing surfaces on the suicide bomber detection problem [1]. The analysis is extended with further examples in this work.

Computational models have been used extensively for analyzing the scattered field patterns around cylindrical objects [2–6]. By careful computational modeling of the electromagnetic scattering of waves in and around a modeled cylinder-based IED geometry, it is possible to predict various features of the expected radar return signal.

2. THE FDFD COMPUTATIONAL METHOD

The nearfield scattering and farfield radiation pattern of an array of six long metal tubes held in place against a flat layer of human tissue with a thin layer of clothing, as shown in Figure 1 [7] is used as a typical example. The scattering is computed for single frequency illumination



Figure 1. Body-worn IED.

by a radar beam using the finite difference frequency domain (FDFD) method. This computational model is similar to the finite element method, but uses the simplified square grid geometry of FDTD [8, 9]. The basic equation used for two dimensional FDFD is the discretized Helmholtz Equation (1).

$$\frac{E_z(i+1, j) + E_z(i, j+1) - 4E_z(i, j) + E_z(i-1, j) + E_z(i, j-1)}{4\Delta} + k^2 = 0, \quad (1)$$

with the standard discretization in terms of spatial step Δ :

$$E_z(x, y) = E_z(i\Delta, j\Delta) \quad (2)$$

FDFD accounts for all multiple scattering effects from each type of medium in the problem geometry: the six 4.4 cm diameter metal cylinders, the polyester cloth holding them in place, and the flesh they are bound to. The geometry is sampled at least as finely as ten points per medium wavelength, capturing most of the fine-scale geometric variations in the problem. The curved surfaces of the cylinders and thin layer of clothing are readily modeled with FDFD. Although it requires solving a system of simultaneous equations, the two-dimensional FDFD method is computationally efficient, with run times on desktop computers on the order of minutes. Three dimensional FDFD is much more computationally intensive, requiring hours of CPU time and GBytes of RAM. As such, 3D FDFD analysis is usually reserved for specific geometries for which the scattering is dominated by variation in all three dimensions. For the current scattering geometry with long metal cylinders and a long, approximately flat human back, much of the farfield scattering information will depend mostly on the variation in the cross section, shown in Figure 2.

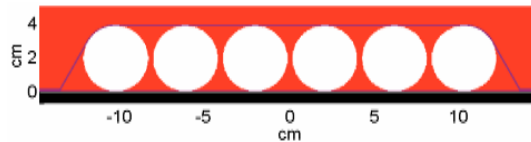


Figure 2. Cross sectional view, from above, of cylindrical explosives on human tissue, held in place with a thin clothing layer.

The total grid size used for this geometry is 159 by 761 points, including the absorbing boundary layer on each of the four sides. The grid cell size is 0.4 mm, which corresponds to 30 points per wavelength in air. Human flesh is modeled as typical high water content tissue, with dielectric constant 27 and conductivity 30 S/m at 25 GHz [10];

polyester clothing is chosen to have dielectric constant 2.8 and loss tangent 0.001 [11]. To avoid reflections at the side of the computational grid, absorbing boundary conditions (ABC) are applied to the exterior grid termination. The ABC used in for this computation is Berenger's Perfectly Matched Layer (PML) [12], chosen to be eight cells deep, with a parabolic conductivity profile. Because the ABC is applied only to the grid termination, and not within the scattering region, the useful scattering region is 143 by 745 cells.

If X is a column vector of stacked E_z values, the discretized Helmholtz equation becomes $AX = B$, with A corresponding to the association between electric field values in space. B is a vector corresponding to excitation of the field with nonzero values only at source positions. In this case, B characterizes the incident plane wave. X is later reshaped to the corresponding geometry, within the 143 by 745 grid in this example.

In order to maintain at least 10 points per medium wavelength over a large computational grid with radar illumination at high frequencies, solving the discretized Helmholtz equation can become cumbersome, requiring more computer RAM and CPU time.

For the geometry considered, there are many points in the scattering region which are perfect electric conductors (PEC). For these regions, the field is known to be of zero magnitude. Because the field value is known in these regions, computational efficiency can be gained by avoiding the calculation of field value within these regions.

The main difficulty in removing these calculations from the two dimensional discretized Helmholtz equation is that the PEC, in this case metal, must be removed from the banded tri-diagonal A matrix without disrupting any information needed for the calculation of the non-metal field values. Another difficulty is in the reconstruction of the final grid with the known values inserted at the correct grid points in the final reconstruction of the nearfield scattering profile.

Removing these calculations greatly decrease the computation time and memory needed find the field values for the entire grid. This enables solving larger problems with the same computational resources.

A. Computational Reduction Applied to Metal (CRAM) Algorithm

To reduce computation time and memory usage, areas of known field value may be omitted during calculation and reintroduced when reconstructing the nearfield radiation patterns. Because the field value for metal objects is always equal to zero, this algorithm can be applied to points within metal objects. A new method is presented below which eliminates unnecessary calculations in metallic regions, speeding up calculations and reducing memory requirements.

First, the cross sectional positions of interior metal points are

identified. Because of the construction of the finite difference equations used to find the field value at any point within the computational grid, the exterior metal points must be retained for calculating the nearby nonmetal field values. The interior points are found by zero padding around the outer edge of the entire geometry grid, and then generating four shifted versions of the cross sectional geometry within this mask: one shifted left, one right, one up, and one down, as shown in Figure 3.

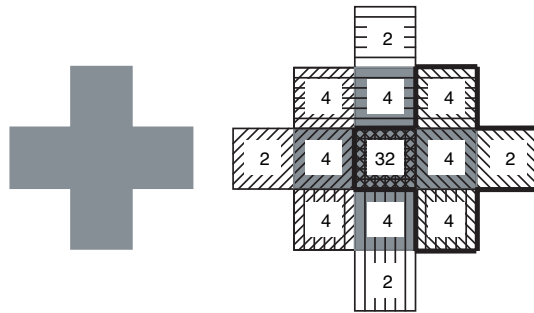


Figure 3. Diagram of method used to identify grid points within a metal object. The original object is shown in gray (left), while four white copies of this object, shown as patterned white objects, are shifted across the grid (right). The right shifted object is highlighted to illustrate this shift. The numbers in the cells indicate the multiplicity of overlap of the metal cell index (2 for no overlap).

The original image is then multiplied by the four shifted versions, and the interior metal points can be identified as having a value of $(metal\ index\ value)^5$. In this way, only the interior metal points are identified, as it is necessary to retain the exterior metal points to compute the scattering off the edge of the metal objects.

Once the indices of the interior metal points are identified, markers are set at these points for subsequent removal of these indices from the matrix equation for the entire grid space.

To remove the interior metal points from the matrix inversion calculation, the corresponding column and row for each metal grid point is removed from the A matrix, and the corresponding row is removed from the column vector B .

Solving the matrix inversion problem $A'X' = B'$ for the new reduced matrices yields the resulting nearfield values for all nonmetal indices. After these values have been computed, the nearfield pattern is reconstructed by using the cross sectional geometry file as a reference for the reinsertion of the zero field values present in the center of metal objects.

Two example cases with different grid sizes are given to demonstrate the computational savings afforded by the CRAM algorithm.

For the 143×741 grid used in this study, the time required for solving the matrix inversion problem was originally 98.3 seconds, with the size of the A matrix equal to 120999×120999 bytes. CRAM reduces this matrix size to 79884×79884 , and the time to compute the solution to the matrix equation to 13.12 seconds, corresponding to savings of 56% in memory and 87% in time.

For a much larger case, a grid size of 286×1491 was used. In this case the A matrix is 426426×426426 bytes, and with no matrix reduction, there is not enough memory in a computer with 1 GB of RAM to compute the solution. With the use of the computational reduction algorithm, the matrix is reduced to 287378×287378 , and inversion can be completed with a run time of 78.2 seconds.

3. RADAR ILLUMINATION

A microwave beam originating from a distant radar source illuminates the geometry viewed from above as shown in Figure 2 as a plane wave, normally incident from the top. The incident field can be decomposed into vertical and horizontal polarizations. The vertical polarization assumes the electric field E_z is perpendicular to the ground, and as such also to the plane of the cross section of Figure 2. This field arrangement, is usually denoted TM, as the magnetic fields are all in the transverse plane of the cross section. For horizontal polarization, the magnetic field H_z is vertical. It is referred to as TE. For the 2D geometry, the entire field distribution is given by either E_z or H_z . This study focuses on the vertical polarization case.

The most efficient procedure for computing scattering in the presence of an infinite half space is to first calculate the specular reflection and transmission of the plane wave on just the half space. The complex Fresnel coefficients are readily available [13]. The incident and reflected fields are used as the background fields in the region above (outside) the flesh interface (shown as a black stripe), while the transmitted field is used as the background inside the flesh. These background fields are then used as excitations multiplying the contrast of the non-air media perturbing the ideal half-space geometry. The scattered fields in the presence of the half space obey the inhomogeneous Helmholtz equation, with non-zero right hand side at field locations in the regions occupied by the cylinders and clothing. The total field is just the sum of the background field and the scattered field.

4. COMPUTATIONAL NEARFIELD SCATTERING

Figure 4 shows the normalized field distribution for the vertical, TM polarized excitation. Here, the scattered and total electric fields E_z and E_T are shown. The greatest scattering occurs between the cylinders rather than off their faces.

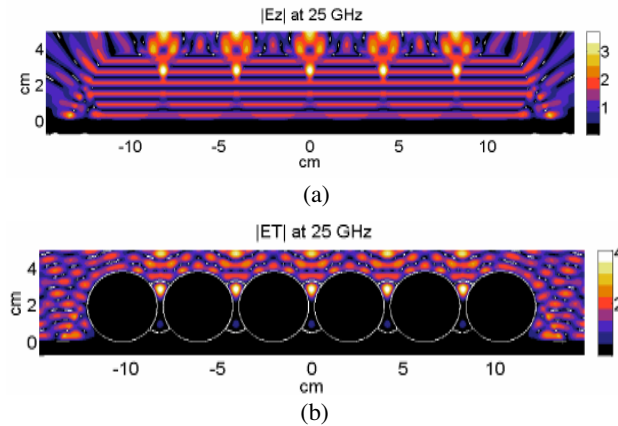


Figure 4. Normalized values for: (a) scattered and (b) total electric fields for the geometry of Figure 2, when illuminated by a normally incident plane wave from above.

Another typical IED geometry was modeled to compare scattering features. In this case, the outer surface of the vest is loaded with nails, often used by suicide bombers as added metallic projectiles to increase the potential damage inflicted. This geometry is given in Figure 5, with nails indicated by small white circles.

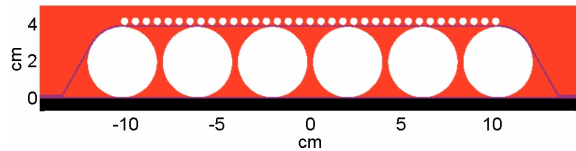


Figure 5. IED cross section with nails adhered to the surface.

The scattered and total field computations for vertical polarization for this geometry are given in Figure 6. The nails clearly have a large effect on both the scattered and total fields. For the TM case, the nails act to shield almost all field between them and the flesh.

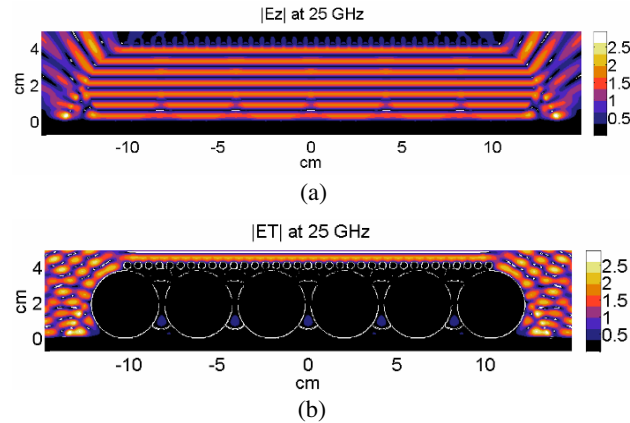


Figure 6. Normalized values for (a) scattered and (b) total electric fields when nails are present as in Figure 5, when illuminated by a normally incident plane wave from above.

The effects of wrinkled clothing have been analyzed by radar at 76 GHz [14], with results showing large variation in measured scattered farfield from wrinkled clothing. This surprising result was reviewed, and the situation modeled for a point of comparison using the FDFD computational model as follows. Two clothing variations — one with tight, small wrinkles and another with looser, larger wrinkles — were added to determine their effects on the nearfield radiation pattern. Each of these models of wrinkled clothing were applied to several cases

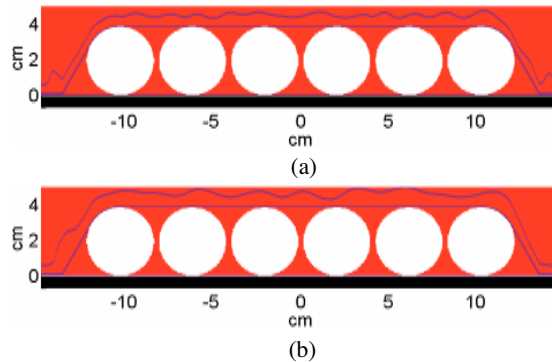


Figure 7. Cross section of IED covered with (a) small wrinkles and (b) large wrinkles.

containing various combinations of human tissue, metal cylinders of explosive materials, fabric enclosure for cylinders, and nails. Examples of these cases are shown in Figure 7.

When wrinkles are present, there is a non-negligible level of clutter added to the nearfield TM pattern, though of lower magnitude than the nearfield pattern for the large metal cylinder and nail cross-sections. Some examples of the total field from this feature are illustrated for the case with six large cylinders and no nails (Figure 8). The scattering effects of the wrinkles appear to increase with the increasing wrinkle amplitude.

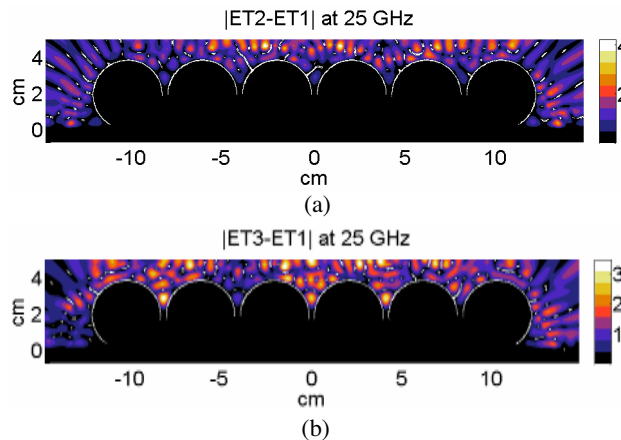


Figure 8. Differences between field magnitude in (a) small and no wrinkles, and (b) large and no wrinkles.

5. FARFIELD PATTERNS OF BODY-WORN IEDS

Converting the computed nearfield scattering values to farfield patterns is accomplished by integrating the electric and magnetic fields times the 2-D Green's function across the four bounding sides of the computational grid, according to Huygens principle [15]. In effect, the entire box is treated as a single scatterer. Next, the farfield approximation is applied to group all distance variation into the single factor e^{-jkr}/r , with only angular variation remaining. For normally incident plane waves, the resulting pattern represents the bistatic radar cross section of the target.

Figure 9 shows the farfield patterns for a ± 35 degree field of view about the backscatter direction, comparing the scattered patterns of

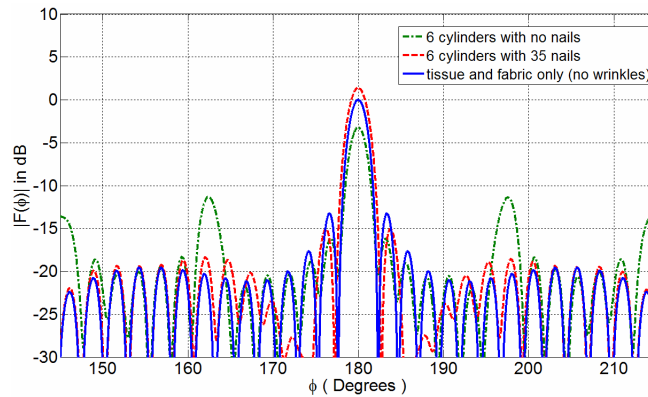


Figure 9. Comparison of scattered farfield radiation patterns for metal cylinder vest, with and without nails.

the body model covered with just smooth clothing, the body model with six metal cylinders (as shown in Figure 2), and the case with both cylinders and 35 nails (Figure 5). Because human flesh is a high water content medium, it scatters strongly at 25 GHz, with a planar reflection coefficient of 0.72. Since the flesh region has a planar interface, it generates strong scattering in the backscatter direction, 180 deg. Despite the total reflection of the perfectly electrically conducting metallic cylinders, the non-planar geometry of the array and 70% smaller width lowers its cross section to levels below that of the body and clothing alone. The cylinder array does have a unique feature in its farfield pattern, that of significant sidelobes at approximately 20 degrees to either side of the main beam. These sidelobes might be used for discrimination of metal cylinder arrays. The addition of nails increases the magnitude of the maximum backscatter, but reduces the characteristic sidelobes in the farfield pattern, indicating that clutter is introduced with the addition of nails.

The effects of wrinkled clothing on both body-only, and body with cylinder cases have been examined. In each case, wrinkled clothing had only a small effect on the magnitude and structure of the farfield patterns. Analysis of the body-only case (Figure 10) shows that added wrinkles decrease the field magnitude at 180 degrees, but cause no large sidelobes as indicated in the metal cylinder case of Figure 9.

The farfield magnitude at 180 degrees is slightly reduced when the metal cylinders are covered with wrinkled clothing, and the sidelobe structure is distorted, but not significantly enough to mask the effects of the reflected fields from the metal objects as illustrated by Figure 11.

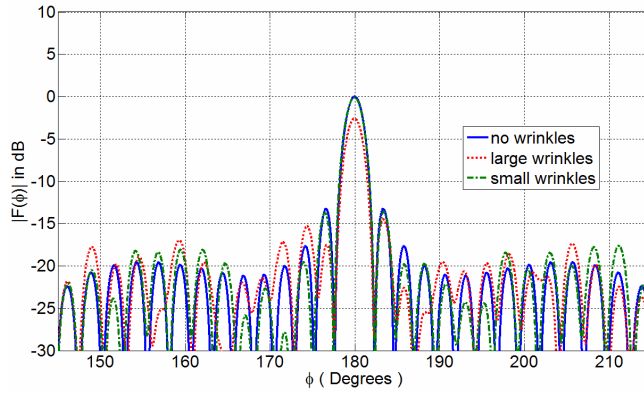


Figure 10. Comparison of scattered farfield radiation patterns for wrinkles of varied intensity covering only flesh.

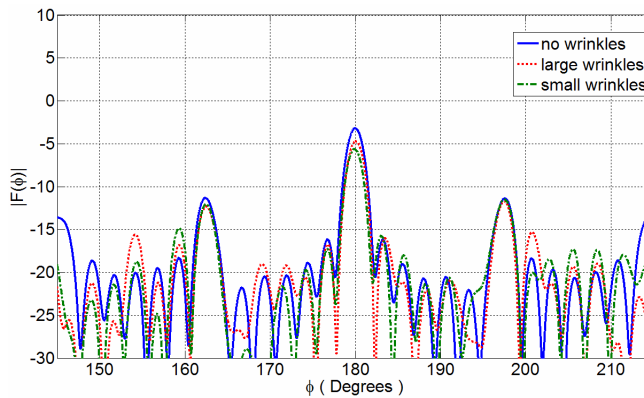


Figure 11. Comparison of scattered farfield radiation patterns with wrinkles of varied intensity covering six metal cylinders.

Because one of the major goals in detection of body-worn IEDs is detection at a safe distance, the relative invariance of the farfield radiation is a clear indicator that the added wrinkled clothing clutter — which generates noticeable scattering in the nearfield patterns — does not lessen detectability of metal cylinders. In addition, the added wrinkles will not significantly alter the sidelobe structure sufficiently to camouflage IEDs (Figure 11), or cause a false alarm for safe individuals (Figure 10).

6. NONUNIFORM CYLINDER SPACING

For all of the previously mentioned cases, it was assumed that the spacing of the cylinders was uniform. The uniform spacing was used to simulate the situation of an IED vest with uniform slots as shown in Figure 1. However, it is to be expected that the exact uniformity of the spacing of the cylinders contributes greatly to the farfield scattering sidelobes at $\pm 18^\circ$ relative to the backscatter direction exhibited in Figures 9 and 11 since the cylinders become, in effect, an array with constructive interference in those directions. In order to examine the influence of the amount of uniformity in the array, the FDFD computational algorithm was implemented for analysis of a cross sectional geometry where the cylinders are spaced at arbitrary intervals (Figure 12).

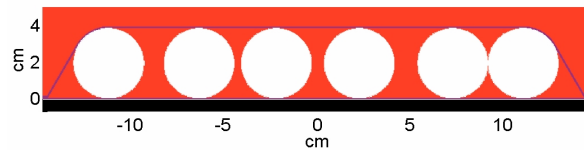


Figure 12. Cross sectional IED geometry for nonuniform spacing of metal cylinders.

Using this geometry yields the farfield pattern shown in Figure 13, after normalization to the case where only human tissue and fabric are present.

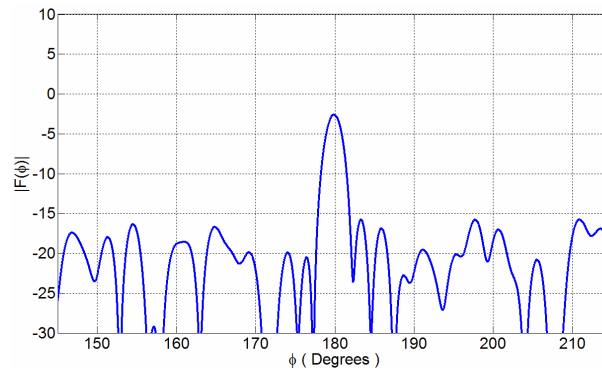


Figure 13. Scattered farfield radiation pattern for nonuniform metal cylinder spacing as normalized to case with no cylinders present.

This image demonstrates that the farfield pattern no longer exhibits the neat, symmetrical pattern with pronounced sidelobes $\pm 18^\circ$ from the backscatter direction as in the previous cases. This matches

the expected outcome, since constructive interference does not occur when the array spacing is uneven.

7. CONCLUSION

Analysis has shown that there are contributions to the nearfield scattered field from the clothing; that the proximity of metal explosive-filled cylinders to each other and to the body is critical; that the addition of nails in the covering layer has great effects on the farfield pattern; and that the farfield backscattered radiation pattern may serve as an important discriminator for uniformly spaced IEDs. However, the intensity of the direct backscattered signal alone is insufficient for discrimination. A tight array of nails adds clutter that distorts the scattering farfield pattern enough to obscure the cylindrical IED array. It has been observed that the addition of wrinkled clothing adds significant clutter to the nearfield patterns, though it contributes much less to the farfield backscatter than does the array of 35 nails. These effects show that the addition of wrinkled clothing would not significantly hinder the radar-based detection of body-worn IEDs at a distance. This study did not consider subject movement, which is likely to occur in practice. Discriminating targets on moving individuals is a more challenging problem and is the subject of further investigation.

ACKNOWLEDGMENT

This work is supported by CenSSIS, the Gordon Center for Subsurface Sensing and Imaging Systems under the ERC Program of the NSF (Award number EEC-9986821), and the Saul and Gitta Kurlat Charitable Foundation. The authors are grateful to the IEEE Microwave Theory and Techniques Society for their support through the undergraduate/pre-graduate scholarship program, and to Ersel Karbeyaz for providing nearfield to farfield conversion software.

REFERENCES

1. Angell, A. and C. Rappaport, "Computational modeling analysis of radar scattering by metallic body-worn explosive devices covered with wrinkled clothing," *IEEE MTT-S International Microwave Symposium Digest*, June 2007.
2. Hamid, A.-K., "Iterative solution to the TM scattering by two infinitely long lossy dielectric elliptic cylinders," *Journal of Electromagnetics Waves and Application*, Vol. 18, No. 4, 529–546, 2004.

3. Norgren, M., "A hybrid FDFD-BIE approach to two-dimensional scattering from an inhomogeneous biisotropic cylinder," *Progress In Electromagnetics Research*, PIER 38, 1–27, 2002.
4. Ciambra, F., "A spectral-domain solution for the scattering problem of a circular cylinder buried in a dielectric half space," *Progress In Electromagnetics Research*, PIER 38, 223–252, 2002.
5. Xu, X.-B. and J. Ao, "A hybrid integral and differential equation method solution of scattering of TM excitation by buried inhomogeneous cylinders," *Progress In Electromagnetics Research*, PIER 15, 165–189, 1997.
6. Hamid, A.-K., "Electromagnetic scattering from a dielectric coated conducting elliptic cylinder loading a semi-elliptic channel in a ground plane," *Journal of Electromagnetics Waves and Application*, Vol. 19, No. 2, 257–269, 2005.
7. <http://www.strategypage.com/gallery/default.asp?target=3.htm&source=suicidebombs>
8. Morgenthaler, A. and C. Rappaport, "Scattering from lossy dielectric objects buried beneath randomly rough ground: Validating the semi-analytic mode matching algorithm with two-dimensional FDFD," *IEEE Trans. on Geoscience and Remote Sensing*, Vol. 39, 2421–2428, November 2001.
9. Rappaport, C., M. Kilmer, and E. Miller, "Accuracy considerations in using the PML ABC with FDFD Helmholtz equation computation," *International Journal of Numerical Modeling*, Vol. 13, No. 471, 471–482, September 2000.
10. Gabriel, S., R. Lau, and C. Gabriel, "The dielectric properties of biological tissues: II. Measurements on the frequency range 10 Hz to 20 GHz," *Phys. Med. Biol.*, Vol. 41, 2251–2269, 1996.
11. Van Hippel, A., *Table of Dielectric Materials*, Wiley, New York, 1953.
12. Berenger, J., "A perfectly matched layer for the absorption of electromagnetic waves," *Journal of Computational Physics*, Vol. 114, No. 1, 185–200, October 1994.
13. Staelin, D., A. Morgenthaler, and A. Kong, *Electromagnetic Waves*, Prentice-Hall, Englewood Cliffs, 1994.
14. Yamada, N., "Radar cross section for pedestrian in 76 GHz band," *R&D Review of Toyota CRDL*, Vol. 39, No. 4, 46–51, 2004.
15. Balanis, C., *Advanced Engineering Electromagnetics*, Wiley, New York, 1989.